IOPscience iopscience.iop.org

Home Search Collections Journals About Contact us My IOPscience

Order–disorder nature of the antiferroelectric transition in Pb_2MnWO_6

This article has been downloaded from IOPscience. Please scroll down to see the full text article.

2009 J. Phys.: Condens. Matter 21 075903

(http://iopscience.iop.org/0953-8984/21/7/075903)

View the table of contents for this issue, or go to the journal homepage for more

Download details:
IP Address: 129.252.86.83
The article was downloaded on 29/05/2010 at 17:56

Please note that terms and conditions apply.

J. Phys.: Condens. Matter **21** (2009) 075903 (9pp) doi:10.1088/0953-8984/21/7/075903

Order–disorder nature of the antiferroelectric transition in Pb_2MnWO_6

G Subías[1,3], J Blasco[1], J García[1], J Herrero-Martín[2] and M C Sánchez[1]

[1] Instituto de Ciencia de Materiales de Aragón, Departamento de Física de la Materia Condensada, CSIC-Universidad de Zaragoza, Pedro Cerbuna 12, E-50009 Zaragoza, Spain
[2] European Synchrotron Radiation Facility, BP 220, F-38043 Grenoble Cedex 9, France

E-mail: gloria@unizar.es

Received 4 November 2008
Published 23 January 2009
Online at stacks.iop.org/JPhysCM/21/075903

Abstract

The nature of the para–antiferroelectric phase transition in Pb_2MnWO_6 was investigated by x-ray absorption spectroscopy. Extended x-ray absorption spectra (EXAFS) and x-ray absorption near-edge structure (XANES) at the Pb L_3-edge, W L_3-edge and Mn K-edge were measured at temperatures above and below the transition temperature, $T_c \sim 445$ K. The temperature dependence of the local geometrical and electronic structure around each of the three atoms was quantitatively determined. XANES spectra confirm the expected formal valence state as Pb^{2+}, W^{6+} and Mn^{2+} both above and below T_c. There are no significant changes of the local structure around the three atoms, which remains distorted in the whole temperature range. This indicates the existence of dynamic local distortions with a short-range order in the paraelectric phase. Below T_c, the local distortions (and the electrical dipoles) are static and their ordered arrangement gives rise to the orthorhombic crystallographic structure. Above T_c, these distortions are dynamically disordered, causing an average cubic crystallographic structure. Hence, the phase transition is of the order–disorder type.

(Some figures in this article are in colour only in the electronic version)

1. Introduction

Since the discovery of ferroelectricity in $BaTiO_3$ [1], a large number of oxides of different structural families (i.e. perovskite, tungsten bronze, boracites, pyrochlore, etc) have been examined in search of new materials for commercial applications (i.e. transducer, computer memory and display, sensors, actuators and electro-optical modulators, pyroelectric detectors, etc). Among them, Pb-based perovskites $Pb_2BB'O_6$ [2] are good candidates because of their high dielectric permittivity. The $6s^2$ lone pair of Pb^{2+} ions and the strong covalent character of Pb–O bonds stabilize a noncentrosymmetric-distorted structure, resulting in spontaneous electric polarization. B is typically a lower valence cation (e.g. Mg^{2+}, Co^{2+}, Ni^{2+}, Zn^{2+}, Sc^{3+} or Fe^{3+}) and B′ is a ferroelectrically active cation with a higher valence and no outer d-electron (e.g. Ti^{4+}, Zr^{4+}, Nb^{5+}, Ta^{5+} or W^{6+}). Depending on the difference in either charge or ionic radii of the B and B′ cations, these materials can be ordered, giving rise to a double perovskite or disordered, where B and B′ cations occupy the same crystallographic site in a simple perovskite [3]. The temperatures and types of the phase transitions in ordered or disordered samples are different: partially or fully disordered compounds undergo smeared ferroelectric phase transitions, which involve relaxation of the dielectric permittivity (so-called ferroelectric relaxors). Ordered compounds exhibit sharper transitions, leading to antiferroelectric-derived phases. Thus, $Pb_2BB'O_6$ constitute the ideal family for studying the microscopic mechanisms of the different types of ferroelectric correlations.

The structural origin of the ferroelectric/antiferroelectric behaviour in these mixed-ion perovskites is still not clear. Ferroelectric as well as other structural phase transitions are often considered in the framework of two limiting mechanisms, namely the displacive-type and the order–disorder mechanisms [4]. Diffraction provides information on the long-range ordered distortions in the ferro-/antiferroelectric phase but only indications about dynamic distortions

[3] Author to whom any correspondence should be addressed.

 © 2009 IOP Publishing Ltd Printed in the UK

(or uncorrelated disorder) in the paraelectric phase (unusually high values of Debye–Waller factors). In other words, using long-range techniques such as diffraction, only the average periodic structure is determined. To identify the mechanisms for this type of transitions, it is necessary to find detailed information about the geometrical structure on the local scale and instantaneous distortions. X-ray absorption fine structure (XAFS) is particularly suitable to provide quantitative information on the geometrical and electronic structure around specific atoms and it provides the partial pair correlation function with high resolution. This makes it ideal for studying mixed crystals such as these lead-based double perovskites. Moreover, since the interaction time for the photoabsorption process is extremely short (of the order of 10^{-16} s), it allows determining the presence of dynamical distortions, i.e. distortions with a lifetime larger than 10^{-16} s. Moreover, the XAFS spectrum is not affected by long-range orientational disorder. Recent XAFS studies suggested that there is a significant order–disorder component in the ferroelectric transition of simple perovskites [5–8], which was in conflict with the prevailing displacive theory. Only a few XAFS studies have been reported so far for complex $Pb_2BB'O_6$ perovskites, most of them related to the disordered relaxor compounds [9–13]. The results show that order–disorder processes may also play an important role in the structural transformations of these compounds.

The present paper is devoted to an experimental study of the para–antiferroelectric phase transition in Pb_2MnWO_6 by XAFS spectroscopy in order to determine the mechanism of the transition. Pb_2MnWO_6 belongs to the ordered lead-based elpasolites (space group $Fm\bar{3}m$) with an ordered arrangement of MnO_6 and WO_6 octahedra sharing corners. Among these compounds are Pb_2CoWO_6 [14], Pb_2CdWO_6 [15], Pb_2MgWO_6 [16] and $Pb_2Mg_{1-x}M_xWO_6$ (M: Mn, Fe, Cu) [17]. Depending on the size of the B^{2+} ion, distorted phases of varied symmetry can be realized by a change in temperature. The phase transition at ∼310 K in Pb_2MgWO_6 separates a high temperature cubic paraelectric phase from a lower temperature orthorhombic antiferroelectric phase whereas in Pb_2CoWO_6 and Pb_2CdWO_6 an incommensurate phase is found below ∼300 K and 683 K, respectively. The transition mechanism in these cases has been concluded as being intermediate between pure displacive and order–disorder [18–20].

Pb_2MnWO_6 undergoes a structural phase transition to an orthorhombic phase (space group, $Pnma$) at $T_c \sim 445$ K [21], resembling the one in Pb_2MgWO_6. This transition is coupled to a sharp change in the dielectric permittivity. Above 445 K, it is paraelectric and presents a first-order phase transition to an antiferroelectric phase below such a temperature. The x-ray crystallographic study of the cubic phase reveals the presence of regular MnO_6 and WO_6 octahedra but with different sizes. The refined W–O bond length is 1.965 Å, which agrees reasonably well with the tabulated ionic radius [22] for W^{6+}–O (1.98 Å). The experimental Mn–O distance is 2.105 Å, smaller than the tabulated datum [22] for Mn^{2+}–O (2.21 Å) but close to the value obtained for related double perovskites. The Pb atoms are located at special positions, occupying the remaining free space with a 12-fold coordination but their temperature factor is very large. This large temperature factor was also found for oxygen atoms. The low temperature orthorhombic phase shows distorted MnO_6 and WO_6 octahedra, mainly due to oxygen shifts. Pb atoms approach four oxygens too, forming a distorted pyramid with them as observed in the related Mg compound [16]. This displacement is coupled to neighbouring Pb atoms giving rise to an antiferrodistortive array in the ac plane.

Despite the detailed study of the crystal structure and properties of this sample [21], several questions are not fully addressed in order to understand the driving force for the transition. First, the large temperature factors for Pb^{2+} and O^{2-} ions in the cubic phase suggest the presence of structural dynamical disorder in this high temperature phase. Second, the large entropy content of the transition, $R \ln 2$, would agree with a significant contribution from an ordering process because transitions driven by displacive mechanisms, either octahedron distortion or tilting, show smaller entropy changes. This value, however, is lower than in related compounds [19, 20], which suggests the presence of either disorder in the low temperature phase or correlated distortions in the high temperature one. Finally, the exact magnitude of the MnO_6 and WO_6 distortions in the antiferroelectric phase deserves further verification using a local technique.

In this paper, we examine the electronic and geometrical local structure around the three metal sites, tracing their temperature changes through the transition at 445 K by XANES and EXAFS spectroscopies. Our results will support an order–disorder structural transition of Pb and W distortions in Pb_2MnWO_6. Dynamic local distortions in the paraelectric phase are both static and ordered in the antiferroelectric phase.

2. Experimental details

A powder sample of Pb_2MnWO_6 was obtained by solid-state reaction using the synthesis procedure described in detail elsewhere [21]. The sample was characterized by x-ray powder diffraction, resulting in almost a single phase. Only a tiny amount of the secondary phase $PbWO_4$ (∼1%) was found. The full characterization of the magnetic, electrical and thermodynamic properties of the phase transition at $T_c \sim$ 445 K was also reported elsewhere [21].

X-ray absorption experiments were performed at the Spanish CRG beamline BM25A at the ESRF (Grenoble, France). The x-rays were monochromatized using an Si(111) double-crystal and harmonic rejection was achieved by 30% detuning of the two crystals from the parallel alignment. EXAFS spectra were measured in transmission using ionization chambers as detectors. Pb L_3-edge and W L_3-edge EXAFS spectra were measured at five temperature points in the range from 300 to 500 K, which covers the paraelectric–antiferroelectric phase transition. Only XANES spectra were recorded at the Mn K-edge at two temperatures, one below and one above the transition, due to the high photoabsorbing matrix. We also recorded XANES and EXAFS spectra at room temperature of metallic Pb and PbO as references for the Pb L_3-edge, metallic W, WO_3 and Ca_2NiWO_6 as references for the W L_3-edge and metallic Mn, MnO, Mn_2O_3 and Pb_2MnReO_6 as references for the Mn K-edge. Pellets were prepared by

dilution with boron nitride and the amount of material was calculated to optimize the expected signal-to-noise ratio at each absorption edge.

XANES spectra were normalized to the high-energy part of the spectrum (∼100 eV beyond the edge) after background removal. EXAFS spectra, $\chi(k)$, were obtained by removing the smooth atomic absorption coefficient (μ_0) by means of a cubic spline fit. The Fourier transform (FT) of the k-weighted EXAFS spectra was calculated as between 2 and 9 Å^{-1} for the Pb L_3-edge and between 2.5 and 11 Å^{-1} for the W L_3-edge using a sine window. The limits for the useful k range are determined by the high temperature data. The intensities of the EXAFS spectra decrease remarkably as the temperature increases and the bad signal-to-noise ratio at large k makes the data no longer useful. The EXAFS structural analysis was performed using the ARTEMIS programme [23], which makes use of theoretical standards calculated by FEFF-6 [24]. The fits to the experimental data were carried out in the R-space fitting mode up to 4.5 Å (first Pb–O and second (Pb–W, Pb–Mn and Pb–Pb) coordination shells). The orthorhombic-distorted crystallographic structure at room temperature was used as a starting model to fit the spectra at all temperatures. The overall amplitude reduction factor S_0^2 was fixed to 1 and the Debye–Waller factors were correlated with the interatomic distances through the Debye function. The internal potential correction (ΔE_0), the Debye temperature (θ_D) and the interatomic distances were the only variables in the fits.

3. Results

3.1. Pb L_3-edge

Figure 1 compares the moduli of the FT of the Pb L_3 k-weighted EXAFS spectra at selected temperatures across the antiferroelectric phase transition. They exhibit the same profiles at all temperatures and the intensity decreases as the temperature increases to a point just above the phase transition, where it remains almost constant. This qualitatively shows that the local structure at the Pb site remains alike in both phases. The FT curves of the Pb L_3 EXAFS spectra for Pb_2MnWO_6 and PbO at $T = 295$ K are compared in the inset of figure 1. There is a clear difference in the first strong peak in the range from 1 to 2 Å, which corresponds to the four O at shorter distances in the PbO_{12} polyhedron of the double perovskite. This peak has much smaller amplitude and a more asymmetric shape than that of the PbO compound, which is tetragonal with four oxygens forming a regular pyramid. This also points out the existence of large local distortions at the Pb site below and above T_c.

In order to obtain quantitative results, we have fitted the spectra using the orthorhombic crystallographic structure at room temperature [21] as a starting model. Seen from the Pb atom, the first oxygen shell (12 O) can be divided into three subshells with four oxygens, each at average distances of 2.569, 2.931 and 3.196 Å (standard deviation among atoms in each shell was lower than 0.06 Å). The second shell, Mn (×4) and W (×4), splits into two with

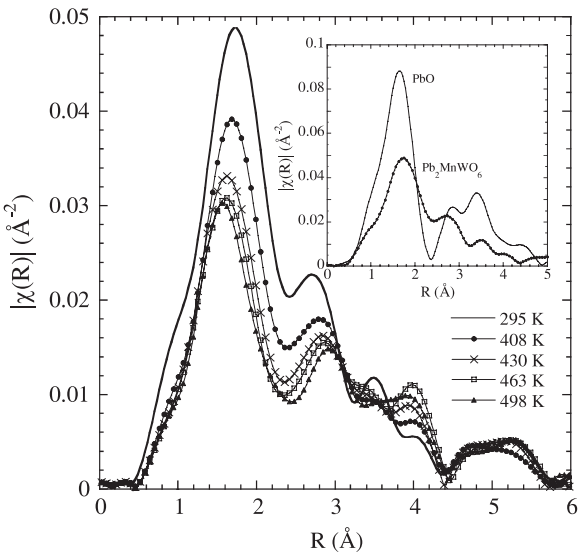

Figure 1. Modulus of the FT of the k-weighted EXAFS data at the Pb L_3-edge at fixed temperatures between room temperature and 500 K (uncorrected for phase shift). Temperatures are indicated in the figure. Inset: comparison of the modulus of the FT (uncorrected for phase shift) of Pb_2MnWO_6 and PbO at 295 K.

two atoms each at average distances of Pb–Mn (Pb–W) of 3.421 (3.408) and 3.661 (3.672) Å. The third coordination shell (Pb) splits into two subshells with three atoms each. This model uses nine structural parameters for the fit. The best fitting results for the different temperatures are presented in figure 2. The obtained interatomic distances at room temperature are in good agreement with those resulting from diffraction techniques [21]. The Pb–O, Pb–Mn, Pb–W and Pb–Pb interatomic distances are nearly independent of temperature, whereas the Debye–Waller factors (σ^2) show a weak temperature dependence, as shown in figure 3. The average σ^2s of the near oxygens and the Mn, W and Pb shells relative to the Pb atom increase with increasing temperature, as expected for a system where local distortions change only slightly and a small discontinuity in the temperature dependence is observed at the phase transition for the three contributions.

We have also checked that the local cubic structure disagrees with the EXAFS data above T_c (paraelectric phase). The fit with the cubic model at the highest temperature (498 K) is much worse. We allowed six variable parameters: E_0, the Debye temperature and the distortion of Pb–O (×12), Pb–Mn (×4), Pb–W(×4) and Pb–Pb (×6) distances. The refined parameters give unphysical values for the Debye–Waller factors. As an example, the σ^2 of the Pb–O distance is 0.098 Å^2, four times larger than that of the distorted model (figure 3).

To clarify the structure of the PbO_{12} polyhedron we employ the pair radial distribution function $P(R)$ as follows:

$$P(R) = \sum_n \frac{N_n}{\sqrt{2\pi\sigma_n^2}} \exp\left(-\frac{(R-R_n)^2}{2\sigma_n^2}\right). \qquad (1)$$

Here the summation is performed over the different Pb–O scattering paths, N_n is the coordination number of oxygen

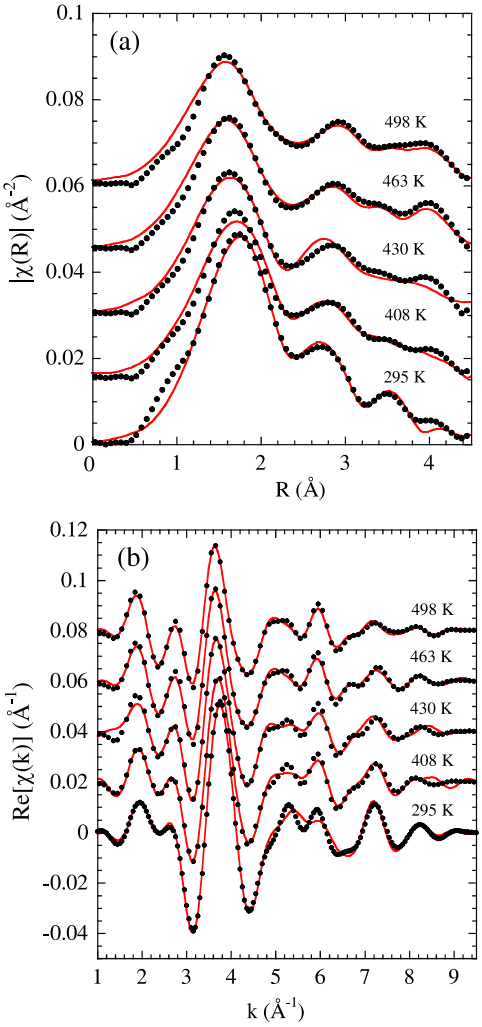

Figure 2. Comparison of the FT of the experimental (closed circles) and best fit (lines, red in e-version) k-weighted EXAFS spectra at the Pb L_3-edge for different temperatures between room temperature and 500 K (uncorrected for phase shift). (a) Modulus and (b) real part.

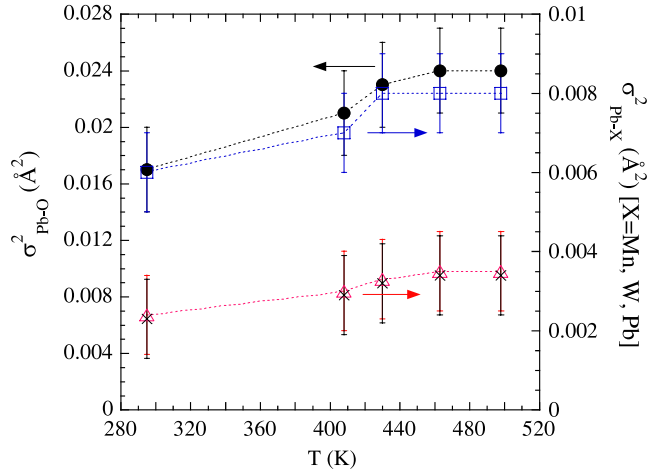

Figure 3. The temperature dependence of the refined Debye–Waller factors (σ^2) for the three coordination shells (closed circles: Pb–O, open squares: Pb–Mn, open triangles: Pb–W, crosses: Pb–Pb interatomic distances). The dashed lines are guides for the eyes.

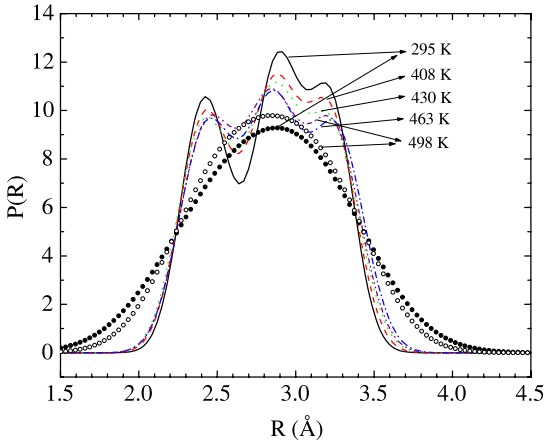

Figure 4. The calculated Pb–O pair radial distribution function ($P(R)$) for different temperatures below and above the para–antiferroelectric transition. Temperatures are indicated in the figure. The Pb–O distance distributions calculated with the average distance and the standard deviation among the O atoms for 295 and 498 K are also shown as closed and open circles, respectively, for comparison.

atoms corresponding to the distance R_n and σ_n^2 is the Debye–Waller factor. The $P(R)$ functions calculated by equation (1) using the fitting results of the first oxygen shell for various temperatures are displayed in figure 4. One can see that the first shell $P(R)$ function is asymmetric and different from a Gaussian distribution (regular PbO_{12} polyhedron) at all temperatures. At room temperature, in the antiferroelectric phase, the peak at the shorter distance side is clearly separated from the other two maxima. As the temperature rises, the $P(R)$ function becomes slightly more symmetric though it still has three well-defined peaks. This shows that Pb is surrounded by high asymmetric oxygen coordination. As this asymmetry is almost temperature-independent, the temperature changes of the total Debye–Waller factor will be very small, as observed in figure 3. With the aim to show this asymmetry, we have also plotted in figure 4 the Pb–O bond distribution calculated with the average distance and the standard deviation of the distribution for 295 and 498 K, as closed and open circles, respectively. It is clear that the width of this Pb–O bond distribution slightly decreases with temperature.

We estimated the average displacements r_0 of the Pb atoms from the centres of the PbO_{12} polyhedrons as $r_0 = \sqrt{\sum_i \langle \Delta x_i^2 \rangle}$, where Δx_i is the displacement of the Pb atom from the centre of the ith O–Pb–O chain (i = 1–6) along this chain and $\langle \Delta x_i^2 \rangle$ is the corresponding mean-square displacement. The average displacement calculated is 0.78 Å, which is independent of temperature. This indicates that Pb atoms are already displaced relative to the oxygen framework above T_c and consequently non-oriented local distortions exist in the cubic phase.

The refined Pb–W interatomic distances are 3.30 ± 0.05 and 3.45 ± 0.05 Å and the corresponding Pb–Mn ones are 3.50 ± 0.06 and 3.80 ± 0.06 Å, in agreement with the low temperature orthorhombic description. Within experimental

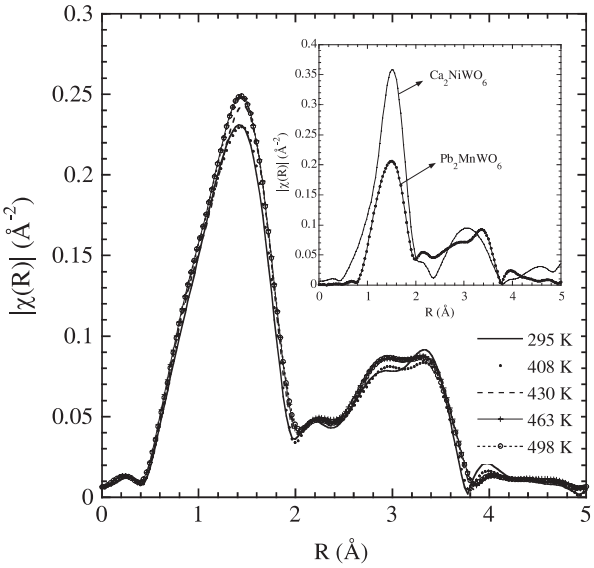

Figure 5. Modulus of the FT of the k-weighted EXAFS data at the W L_3-edge at fixed temperatures between room temperature and 500 K (uncorrected for phase shift). Temperatures are indicated in the figure. Inset: comparison of the modulus of the FT (uncorrected for phase shift) of Pb_2MnWO_6 and Ca_2NiWO_6 at 295 K.

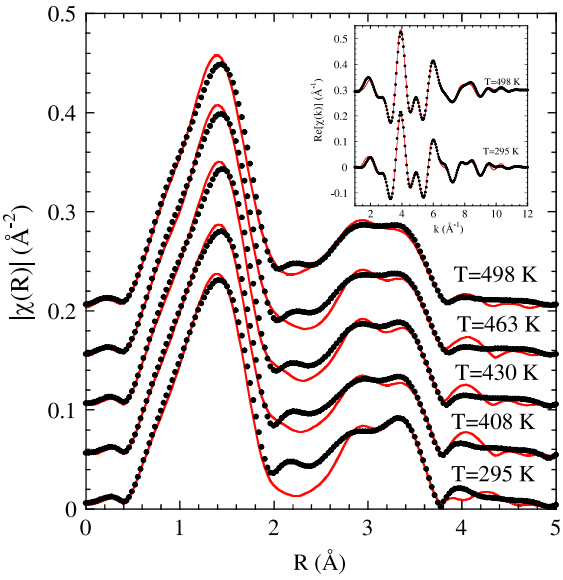

Figure 6. Comparison of the modulus of the FT of the experimental (closed circles) and best fit (lines, red in e-version) k-weighted EXAFS spectra at the W L_3-edge for different temperatures between room temperature and 500 K (uncorrected for phase shift). Inset: experimental (closed circles) and best fit (lines, red in e-version) real parts of the FT at 295 K ($T < T_c$) and 498 K ($T > T_c$).

error, the distances do not change with temperature. The results show that two W atoms are closer to the Pb centre along the W–Pb–Mn chain whereas the two corresponding Mn atoms are far away. The off-centre displacement of this second shell relative to the Pb atom is $r_0 = 0.37$ Å, different from the one of the first oxygen shell. This means that the W and Mn atoms could also be displaced relative to their oxygen octahedra. The occurrence of these distortions will be discussed later from the W L_3-edge and Mn K-edge EXAFS results.

According to these results, the changes in macroscopic symmetry reported by diffraction have no impact on the local structure around the Pb atom, which is distorted both in the low temperature orthorhombic and in the high temperature cubic phases. These local distortions agree with the fact that Pb atoms are displaced from the corresponding oxygen planes of the ideal cubic PbO_{12} polyhedron. Moreover, both the Pb–O bond length distribution and the magnitude of the displacement do not significantly change through the phase transition point.

3.2. W L_3-edge

The local geometrical structure of the WO_6 octahedron was studied by W L_3 EXAFS spectroscopy. The moduli of the FT of the k-weighted EXAFS spectra for different temperature values are shown in figure 5. No significant temperature dependence is detected for R values up to 5 Å. The inset in figure 5 compares the FT of the W L_3 EXAFS for Pb_2MnWO_6 and Ca_2NiWO_6 samples at 295 K. We can see that the first peak of the FT, at R values lower than 2.5 Å, differs significantly between the Pb-based and the Ca-based double perovskites. In the latter, the first neighbours of a W atom are six oxygen atoms forming a regular octahedron at a distance of 1.92 ± 0.02 Å. The decrease in the intensity of the first oxygen coordination peak in the Pb-based double perovskite gives evidence for the existence of a distribution of the W–O distances in this compound. This distribution is temperature-independent within experimental accuracy.

The spectra were fitted, as in the case of the Pb L_3 EXAFS, using the room temperature orthorhombic structure. The FT of the k-weighted EXAFS spectra are shown in figure 6 with overlaid fitted curves (solid lines). Examples of the real part of the experimental data and the fitting results are shown in the inset of figure 6. The data do not display qualitative differences with increasing temperature from far below to above the phase transition. Seen from the W atom, the first shell can be split into three subshells. Two of the O atoms lie slightly offset from the b axis (1.945 Å) and the other four are in the plane perpendicular to the b axis. The average distance of two of these oxygens from the W atom is 2.028 Å and the other two are at 1.772 and 2.165 Å, respectively. The values of the refined parameters confirm a highly distorted WO_6 octahedron at all temperatures, including the cubic phase that roughly corresponds to five short distances at $\sim 1.89 \pm 0.03$ Å and another quite long one (2.28 ± 0.08 Å).

The temperature dependence of the first oxygen shell pair distribution function $P(R)$ calculated using equation (1) is displayed in figure 7 and compared to Ca_2NiWO_6. The first shell $P(R)$ function at room temperature is close to a Gaussian for the regular WO_6 octahedron in Ca_2NiWO_6, whereas it has two clear maxima in agreement with the $5 + 1$ distribution of distances for Pb_2MnWO_6. This asymmetric function remains almost constant up to 500 K but the average W–O distance slightly increases as the temperature rises, showing a small expansion of the octahedron. The Debye–Waller factor is temperature-independent (see the inset of figure 7).

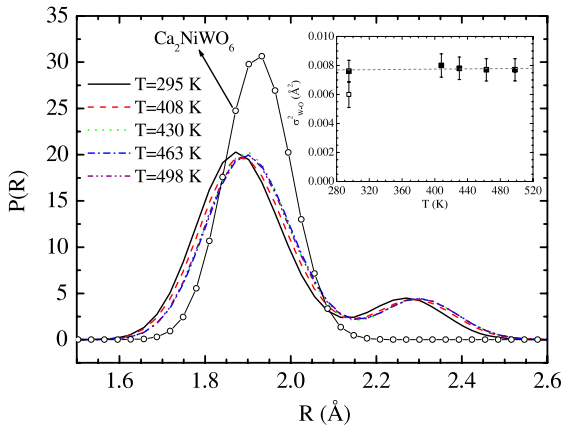

Figure 7. The calculated W–O pair radial distribution function ($P(R)$) for different temperatures below and above the para–antiferroelectric transition. Temperatures are indicated in the figure. The calculated W–O pair radial distribution function ($P(R)$) for Ca_2NiWO_6 at 295 K is also shown for comparison. Inset: the temperature dependence of the refined Debye–Waller factors (σ^2) for the first coordination shell (W–O bond). The dashed line is a guide for the eyes.

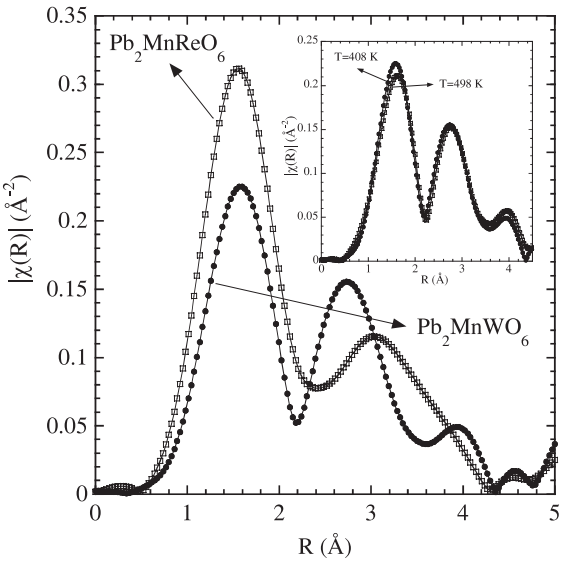

Figure 8. Comparison between the modulus of the FT of the k-weighted EXAFS data at the Mn K-edge of Pb_2MnWO_6 and Pb_2MnReO_6 at 295 K. Inset: modulus of the FT of Pb_2MnWO_6 at 408 K ($T < T_c$) and 498 K ($T > T_c$).

Therefore, the W atoms are not located at the centre of inversion in the oxygen octahedron both below and above the transition temperature.

3.3. Mn K-edge

The Mn K EXAFS was very noisy and the useful range in the photoelectron wavenumber k was 6.5 $Å^{-1}$. Therefore, only a qualitative analysis of the first oxygen shell was carried out. Figure 8 compares the moduli of the FT of the Pb_2MnWO_6 k-weighted XAFS spectra at room temperature with Pb_2MnReO_6. This comparison shows that, for Pb_2MnWO_6, the intensity of the first peak at 1.6 Å is smaller than that of the Re double perovskite, where Mn has a quite regular oxygen environment. This result indicates that the MnO_6 octahedron is distorted in the W double perovskite. This local distortion of the MnO_6 octahedron in Pb_2MnWO_6 is also nonzero above the transition, as deduced from the inset of figure 8, where the qualitative comparison of the moduli of the FT at 408 and 498 K shows that they are similar to each other.

To determine the kind of distortion for the Mn atoms, we have fitted the data for the first shell from 1 to 2 Å using the orthorhombic structure. According to the results, Mn is only slightly shifted from its corresponding centre of inversion position, giving two sets of Mn–O bonds with lengths equal to 2.23 ± 0.05 Å ($\times 4$) and 2.03 ± 0.05 Å ($\times 2$).

3.4. XANES

Normalized XANES spectra as a function of temperature at the Pb L_3-, W L_3-and Mn K-edges are shown in figure 9. At the Pb L_3, there is a continuous evolution in the spectral shape with increasing temperature up to T_c, though the differences observed are very small (see figure 9(a)). No chemical shift is observed between 295 and 498 K. Therefore, the local electronic and geometrical structure around Pb barely changes across the antiferroelectric phase transition, in line with the EXAFS analysis. The Pb L_3 XANES of the double perovskite is compared to those of the metallic Pb and PbO oxide (Pb^{2+}) in the inset of figure 9(a). We find that the edge position for this double perovskite lies very close to that for the divalent Pb oxide and none of them show the prepeak feature typical of PbO_2 due to the effect of vacant 6s orbitals [25]. This suggests that the unoccupied electronic structure in this material is dominated by the local square pyramidal coordination around Pb, which is similar to the PbO_4 polyhedron in PbO and it appears from the covalent nature of the Pb–O bonding with the $6s^2$ lone pair.

Normalized XANES spectra at the W L_3-and Mn K-edges at higher temperatures and at room temperature are presented in figures 9(b) and (c), respectively. The spectra above and below T_c are alike for both transition-metal absorption edges. In both cases, the spectra can be superimposed without noticeable changes, indicating that the local electronic structures of W and Mn atoms do not change in the paraelectric to antiferroelectric transition. The W L_3 XANES of the Pb-based double perovskite is compared to those of the WO_3 oxide and Ca_2NiWO_6 reference samples with the W^{6+} (d^0) ion in the inset of figure 9(b). The experimental W L_3-edge XANES spectrum consists of a prominent peak, the so-called white line, just above the absorption edge. The position of the white-line maximum and the area are practically the same for all the samples, in agreement with the presence of W^{6+}. The most striking difference is in the shape of the spectra. A uniformly broad peak with an FWHM (full width at half-maximum) of ~8 eV is observed in WO_3. For Ca_2NiWO_6 and Pb_2MnWO_6, the FWHM of the white line is the same as for the binary oxide WO_3, in agreement with an octahedral coordination for the three samples but two peaks are observed in the white line. These differences in the shape of the white line are interpreted as being due to splitting of the W 5d states

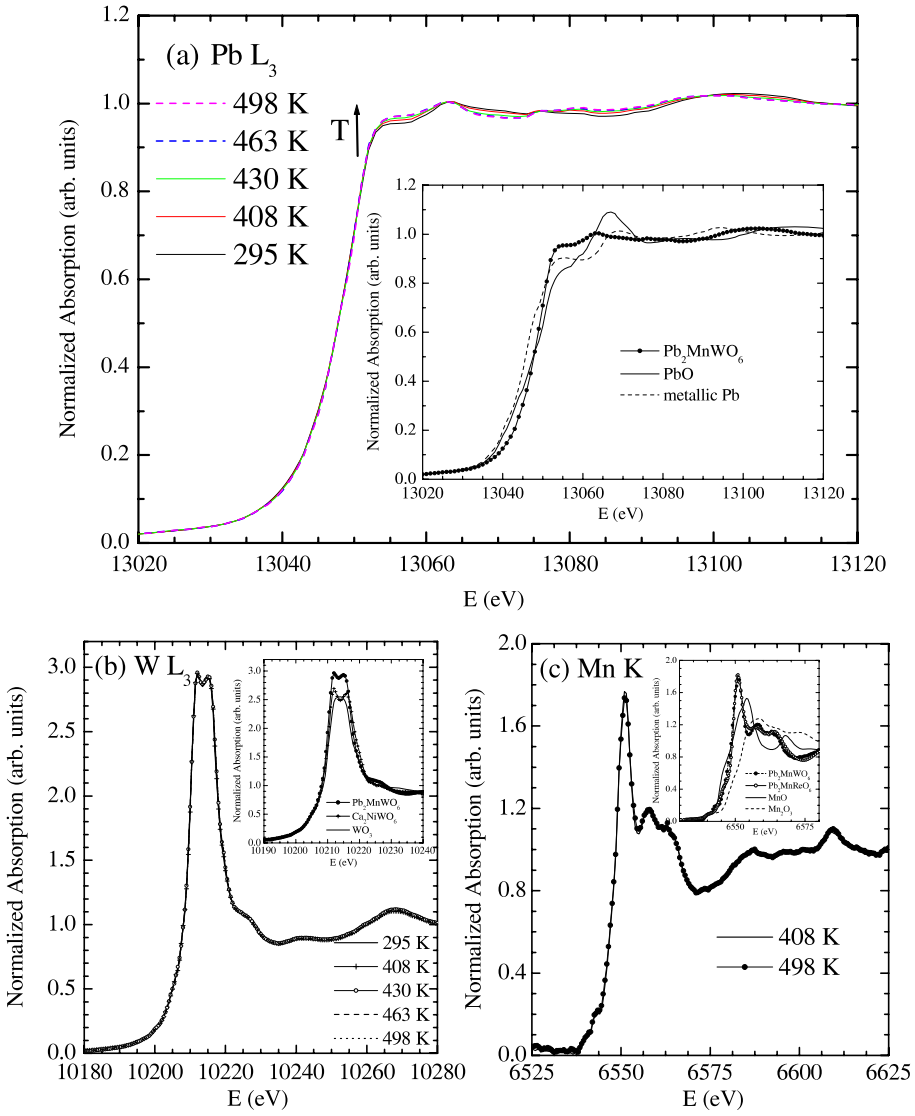

Figure 9. Normalized XANES spectra for Pb_2MnWO_6 for different temperatures (a) at the Pb L_3-edge, (b) at the W L_3-edge and (c) at the Mn K-edge. Temperatures are indicated in the figures. Insets compare the normalized XANES spectrum for Pb_2MnWO_6 at 295 K with (a) XANES spectra for metallic Pb and PbO reference compounds at the Pb L_3-edge, (b) XANES spectra for WO_3 and Ca_2NiWO_6 reference compounds at the W L_3-edge and (c) XANES spectra for MnO, Mn_2O_3 and Pb_2MnWO_6 reference compounds at the Mn K-edge.

by the ligand field, which depends on the structural distortion of the octahedral symmetry [26]. Therefore, Ca_2NiWO_6 with regular octahedral WO_6 units have the largest splitting with a value of 5 eV (as deduced from the second derivatives of the W L_3-edge XANES spectra) whereas the distorted octahedral structure of WO_3 leads to a small splitting of 4 eV. The energy gap of the two split bands in the Pb-based double perovskite is 4.5 eV, which falls in the middle. This suggests the presence of distorted octahedral WO_6 units in this perovskite, supporting the EXAFS results.

The Mn K-edge XANES of Pb_2MnWO_6 is compared to those from the Pb_2MnReO_6-related perovskite and binary oxides MnO and Mn_2O_3 with formal Mn^{2+} and Mn^{3+} ions, respectively, in the inset of figure 9(c). At the Mn K-edge, the main difference among XANES spectra concerns the energy position of the absorption edge that is mainly ascribed to the formal Mn oxidation state. XANES spectra for the two Pb-based double perovskites are very similar to each other in agreement with their having very similar crystallographic structure. Their absorption edges are located close to that of MnO, certifying that the Mn oxidation state is 2+ in both compounds.

4. Discussion and conclusions

In this paper we presented an XAFS study of the paraelectric–antiferroelectric phase transition in Pb_2MnWO_6. Pb, W and Mn x-ray absorption edges were used. Direct quantitative information on the local structure surrounding the three atoms was obtained and it can be summarized in four points.

(1) Locally unit cells remain orthorhombic even above $T_c \sim$ 445 K and the local distortions do not change over the entire temperature range.

(2) The Pb atoms are displaced from the corresponding oxygen planes from the cubic perovskite structure in the [100] direction below and above the transition temperature. The pair radial distribution function is asymmetric and it shows a peak at the shorter distance side clearly separated from the other two maxima at room temperature. Such a Pb atom shift results in four short Pb–O bonds with a mean bond distance of 2.42 ± 0.02 Å, leading to a PbO_4 pyramidal configuration as in PbO. This pyramidal configuration around Pb is almost independent of temperature.

(3) The W atoms are also displaced relative to the oxygen octahedra below and above the transition temperature. This displacement varies little with temperature. The local atomic structure of the WO_6 octahedra agrees with five short distances at $\sim 1.89 \pm 0.03$ Å and another quite long one at 2.28 ± 0.08 Å. On the other hand, a larger MnO_6 octahedron is deduced with a mean bond distance of 2.16 ± 0.05 Å. Although the displacement of Mn relative to the oxygen shell is rather small, it also exhibits a distorted octahedral coordination that does not display any noticeable temperature change.

(4) XANES spectra at temperatures below and above the transition confirm the expected oxidation states as Pb^{2+}, W^{6+} and Mn^{2+}.

In summary, the local geometrical structure of Pb_2MnWO_6 is alike in both paraelectric and antiferroelectric phases, showing that the dipoles produced by atomic shifts (Pb and W) from their corresponding inversion centres are already present in the paraelectric phase. The apparent contradiction between the crystallographic description (Pb, Mn and W atoms in a centre of symmetry) and the XAS results can be easily reconciled. XAS spectroscopy provides information on the short-range structure around a specific atom in a very short time (lower than 10^{-16} s). Therefore, the paraelectric phase would be described as an ordered array of uncorrelated distorted units. Only the average local structure is periodically ordered, giving rise to the observed cubic diffraction pattern. As these distortions are ordered (and static) in the orthorhombic antiferroelectric phase, they must be dynamically disordered above T_c. In this sense, the antiferroelectric–paraelectric phase transition can be classified in the order–disorder type.

As has been reported in [21], the antiferroelectric phase can be described as antiferrodistortive couples of pyramidal Pb environments along the c axis. This study reveals that these pyramids are already present in the paraelectric phase, showing a type of short-range ordering that should be larger than one individual pyramid. These correlated blocks are then dynamically disordered. Our EXAFS results show that the local geometrical structure remains unaltered up to 5 Å, a distance larger than one unit formula. This result can also explain the strong but limited entropy content of the transition. If we assumed that the ordered unit is the unit formula, we would get an entropy content of about $R \ln 6 = 1.79R$ (six possible orthorhombic domains). On the other hand, if the ordered unit includes one orthorhombic unit cell with $Z = 4$, the expected entropy content would be $1/4R \ln 6 = 0.448R$. The experimental entropy content was 0.73 R [21] so the comparison indicates that the disordered units are smaller than the orthorhombic unit cell dimension but larger than the dimension of one unit formula. This nicely agrees with the XAFS description, showing that the metal-distorted sites are strongly correlated in the paraelectric phase.

Finally, the presence of local distortions above T_c has been recently observed in other transition-metal oxides undergoing structural phase transitions coupled to electrical or magnetic ones [27, 28]. It has been shown that all such transitions have an essential element of order–disorder of the local distortions by long-range interactions. Then, the order–disorder nature seems to be a common behaviour for this type of phase transition in highly correlated metal oxides when structural, electric and magnetic degrees of freedom are coupled.

Acknowledgments

Financial support from the Spanish CICyT (projects no. MAT 05-04562 and FIS2008-03951) and Diputación General de Aragón (DGA-CAMRADS) are gratefully acknowledged. The authors thank ESRF for granting beam time and the staff from the Spanish CRG beamline BM25 for their kind assistance during the experiment.

References

[1] Wul B and Goldmann L M 1945 *C. R. Acad. Sci. USSR* **46** 139
[2] Gagulin V V, Fadeeva N V, Belous A G, Sevastianova L A, Titov A V, Pltnikova M V, Mitrofanov K P, Zubova E V, Solovev S P and Venevtsev Yu N 1977 *Phys. Status Solidi* a **44** 247
[3] Galasso F S 1990 *Perovskites and High T_c Superconductors* (New York: Gordon and Breach)
[4] Lines M E and Glass A M 1977 *Principles and Applications of Ferroelectrics and Related Materials* (Oxford: Clarendon)
[5] de Mathan N, Prouzet E, Husson E and Dexpert H 1993 *J. Phys.: Condens. Matter* **5** 1261
[6] Stern E A and Yacoby Y 1996 *J. Phys. Chem. Solids* **57** 1449
[7] Shuvaeva V A, Yanagi K, Yagi K, Sakaue K and Terauchi H 1998 *Solid State Commun.* **106** 335
[8] Ravel B, Stern E A, Vedrinskii R V and Kraizman V L 1998 *Ferroelectrics* **206** 407
[9] Prouzet E, Husson E, de Mathan N and Morell A 1993 *J. Phys.: Condens. Matter* **5** 4889
[10] Li P, Wang Y and Chen I W 1994 *Ferroelectrics* **158** 229
[11] Chen I W, Li P and Wang Y 1996 *J. Phys. Chem. Solids* **57** 1525
[12] Matsushima Y, Ishizawa N, Wakiya N and Mizutami N 2000 *J. Ceram. Soc. Japan* **108** 617
[13] Shuvaeva V A, Pirog I, Azuma Y, Yagi K, Sakaue K, Terauchi H, Raevskii I P, Zhuchkov K and Antipin M Yu 2003 *J. Phys.: Condens. Matter* **15** 2413
[14] Bonin M, Paciorek W, Schenk K J and Chapuis G 1995 *Acta Crystallogr.* B **51** 48
[15] Sciau Ph and Grabille D 1995 *Aperiodic'94* ed G Chapuis and W Paciorek (Singapore: World Scientific) p 460
[16] Baldinozzi G, Sciau Ph, Pinot M and Grabille D 1995 *Acta Crystallogr.* B **51** 668
[17] Barbur I and Ardelean I 2001 *Phase Transit.* **74** 367
Barbur I, Ardelean I, Borodi G, Veres A and Cete Z 2003 *Mater. Lett.* **57** 1327
[18] Baldinozzi G, Sciau Ph and Bulou A 1995 *J. Phys.: Condens. Matter* **7** 8109

[19] Flerov I N, Gorev M V and Sciau Ph 2000 *J. Phys.: Condens. Matter* **12** 559
[20] Gorev M V, Flerov I N, Bondarev V S and Sciau Ph 2002 *Phys. Solid State* **44** 353
[21] Blasco J, Merino R I, García J and Sánchez M C 2006 *J. Phys.: Condens. Matter* **18** 2261
[22] Shannon R D 1976 *Acta Crystallogr.* A **32** 751
[23] Ravel B and Newville M 2005 *J. Synchrotron Radiat.* **12** 537
[24] Rehr J J and Albers R C 2000 *Rev. Mod. Phys.* **72** 621
[25] Yu Y H, Tyliszczak T and Hitchcock A P 1990 *J. Phys. Chem. Solids* **51** 445
[26] Yamazoe S, Hitomi Y, Shishido T and Tanaka T 2008 *J. Phys. Chem.* C **112** 6869
[27] Sánchez M C, Subías G, García J and Blasco J 2003 *Phys. Rev. Lett.* **90** 045503
[28] Subías G, García J and Blasco J 2005 *Phys. Rev.* B **71** 155103